Available online at www.sciencedirect.com
SCIENCE DIRECT®
PERGAMON
Computers and Structures 81 (2003) 1783–1794
Computers & Structures
www.elsevier.com/locate/compstruc

The partition of unity quadrature in element-free crack modelling

A. Carpinteri, G. Ferro, G. Ventura *

Department of Structural and Geotechnical Engineering, Politecnico di Torino, Corso Duca degli Abruzzi 24, 10129 Torino, Italy

Received 14 January 2002; accepted 14 February 2003

Abstract

One of the most promising application of element-free methods is the ability of analyzing crack propagation problems without the necessity of remeshing the model as the crack advances. Moreover the possibility of enriching the classical polynomial basis, introducing some integrals of the Westergaard's solution, make the near crack tip solution accurate without requiring a very fine discretization or special treatment. In the paper the crack propagation problem is numerically analyzed by a new approach in computing the equilibrium equations. In this approach the quadrature of the variational form is not realized by introducing a background cell structure, as commonly done in literature, but by a mesh-free approach based on the partition of unity property of the shape functions. Some numerical examples illustrate the effectiveness of the method.
© 2003 Civil-Comp Ltd. and Elsevier Ltd. All rights reserved.

Keywords: Meshless; Element free; Crack propagation; Quadrature

1. Introduction

Meshless and in general partition of unity methods are receiving attention in computational mechanics research because of some advantages they have compared to the classical finite element method, namely higher rates of convergence, ability to model discontinuities by basis enrichment, insensitivity to distortion in large displacement problems, construction of solutions with any desired degree of continuity. Details on the partition of unity method can be found in [1].

In these methods the discretization is purely nodal, and the finite element concept of connectivity between elements is not introduced. Consequently only a cloud of nodes needs to be generated, and local refinement is made increasing the node density in the region of interest. Given the shape functions constructed on a given nodal arrangement, the weak form of the equilibrium equations (or in general the variational principle for the problem under consideration) require quadratures over the domain. This is a major task in the application of these methods. In fact the shape functions are very complex compared to the finite element ones and they are therefore much difficult to integrate. Different approaches have been used:

- introduction of integration cells in the domain, i.e. of an underlying mesh used only for the quadrature;
- nodal integration approaches, requiring proper modifications of the variational principle [2,3];
- modification of the variational principle from a global to a series of local ones restricted to the support of the weight functions [4,5].

In the paper a new and different approach is introduced [6,7], based on the partition of unity property of the shape functions stating that the sum of the shape functions at any point is equal to 1. Introducing the sum of the shape functions as a unit weight in the quadrature of the variational form, the quadrature over the whole

* Corresponding author.
E-mail address: giulio.ventura@polito.it (G. Ventura).

0045-7949/03/$ - see front matter © 2003 Civil-Comp Ltd. and Elsevier Ltd. All rights reserved.
doi:10.1016/S0045-7949(03)00202-5

domain can be transformed into a sum of integrals over the weight function supports. The general problem of the quadrature over the whole domain is therefore converted into the sum of integrals over a standard domain which is generally a square or a circle, depending on the choice of the support of the weight functions.

This method, called here partition of unity quadrature (PUQ) does not require therefore the subdivision of the whole domain into smaller integration cells and the modification of the variational principle is not needed. Moreover its range of applicability is not limited to meshless methods, but it can be seen as a general approach for computing integrals over arbitrary domains.

The crack propagation problem has been analyzed in literature [8] using standard cell quadrature, while nodal integration [2], modified variational principles [4,5] and partition of unity quadrature [6,7] have actually been applied on patch tests and on some classical benchmark problems. In the analysis of cracks cell quadrature requires, at each crack tip advancement, the redefinition of the integration cells and Gauss points around the tip. The paper investigates the application of the partition of unity quadrature in crack problems, and compares the stress intensity factors evaluation results obtained by the PUQ against the classical integration on subcells.

2. Moving least squares approximation

In this section the approximation of a scalar function $\delta(x)$ in a domain Ω is considered. The MLS approximation uses a set of nodal points, a set of weight functions, and a set of basis functions. At each point of the domain the function is approximated by a linear combination of the basis functions. Within the domain, a set of nodes $x_I, I = 1, \ldots, N$, is considered, Fig. 1, and the parameter associated with the approximation at node I is denoted by δ_I. The coefficients for the basis functions in this linear combination differ from point to point. They are computed by a moving least squares approximation for the function under consideration. In order to obtain the coefficients for the basis functions a system of equations has to be solved at each point of the domain.

A weight function $w_I = w(x - x_I)$ with compact support is associated to each node of the domain. Let Ω_I be the support associated to w_I; w_I reaches the maximum value for $x = x_I$, it is non-negative, monotonically decreasing and such that $w_I = 0$, $\forall x \in \partial\Omega_I$. The support is generally circular or rectangular and then the weight function assumes the shape of a ball-function, one for each discretization node x_I. Generally, polynomial or exponential function are used [9].

The moving least-square approximation $\eta(x)$ of the function $\delta(x)$ in the domain Ω as a linear combination of basis functions $\{p(x)\}$ is given by:

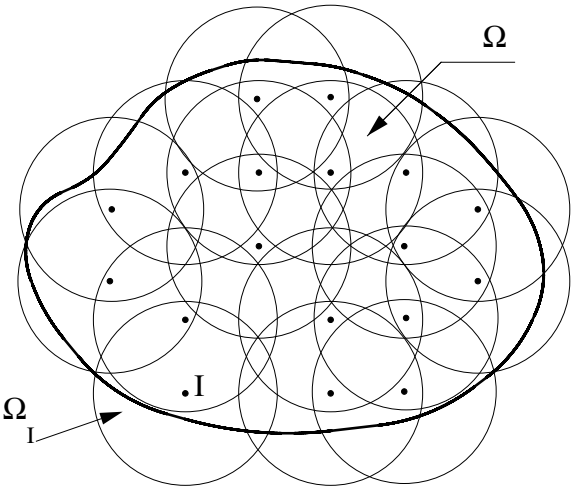

Fig. 1. A computational model for MLS approximation showing the boundary, the nodes and the weight function supports.

$$\eta(x) = \sum_{i=1}^{m} p_i(x) a_i(x) = \underset{(1\times m)}{\{p(x)\}^{\mathrm{T}}} \underset{(m\times 1)}{\{a(x)\}}, \tag{1}$$

where m is the number of the terms in the basis and $\{a(x)\}$ is the vector of the coefficients which are functions of the spatial coordinates x. The choice of the basis depends on the problem to be solved. In particular, any function included in the basis can be reproduced exactly by the MLS approximation. Therefore the introduction of integrals for a particular boundary value problem enhances the convergence rate. A typical example is given by the $\sqrt{r}$ function in the linear elastic fracture mechanics problem, r being the distance from the crack tip. The most common linear and quadratic bases are reported in Table 1.

At any point x the coefficients $\{a(x)\}$ are obtained by minimizing the square of the difference between the local approximation $\eta(x)$ and the value δ_I of the function $\delta(x)$ for $x = x_I$. Therefore the following functional is considered:

$$J(x) = \frac{1}{2} \sum_{I=1}^{n} w_I(x - x_I) \left[\sum_{i=1}^{m} p_i(x_I) a_i(x) - \delta_I \right]^2, \tag{2}$$

Table 1
Typical polynomial bases for MLS approximation

	1D	2D
Linear basis	$\{p(x)\}^{\mathrm{T}} = \{1, x\}$	$\{p(x)\}^{\mathrm{T}} = \{1, x, y\}$
Quadratic basis	$\{p(x)\}^{\mathrm{T}} = \{1, x, x^2\}$	$\{p(x)\}^{\mathrm{T}} = \{1, x, y, xy, x^2, y^2\}$

where $w_I = w(x - x_I)$ is the weight function for the node I and n is the number of the nodes whose supports contain the point x. In fact it can be noted that, as the weight functions have a compact support, the sum over I is limited to the nodes for which the associated weight function has the property $x \in \Omega_I$. Thus the presence of the weight function makes the functional J defined over a set of neighbor nodes $n \ll N$ and localizes the moving least square interpolation.

Eq. (2) can be rewritten in matrix form:

$$J(\{a(x)\}) = \frac{1}{2}\left(\underset{(n\times m)}{[P]}\ \underset{(m\times 1)}{\{a(x)\}} - \underset{(n\times 1)}{\{\delta\}}\right)^{\mathrm{T}} \underset{(n\times n)}{[W(x)]} \times \left(\underset{(n\times m)}{[P]}\ \underset{(m\times 1)}{\{a(x)\}} - \underset{(n\times 1)}{\{\delta\}}\right), \tag{3}$$

where $\{\delta\}^{\mathrm{T}} = \{\delta_1, \delta_2, \ldots, \delta_n\}$, is the vector of function values at the nodal points. $[P]$ has the following form:

$$\underset{(n\times m)}{[P]} = \begin{bmatrix} p_1(x_1) & p_2(x_1) & \cdots & p_m(x_1) \\ p_1(x_2) & p_2(x_2) & \cdots & p_m(x_2) \\ \cdots & \cdots & \cdots & \cdots \\ p_1(x_n) & p_2(x_n) & \cdots & p_m(x_n) \end{bmatrix}, \tag{4}$$

and $[W(x)]$ is provided by:

$$\underset{(n\times n)}{[W(x)]} = \begin{bmatrix} w(x-x_1) & 0 & \cdots & 0 \\ 0 & w(x-x_2) & \cdots & 0 \\ \cdots & \cdots & \cdots & \cdots \\ 0 & 0 & \cdots & w(x-x_n) \end{bmatrix}. \tag{5}$$

In order to find the coefficients $\{a(x)\}$, the extremum of J must be determined:

$$\underset{(m\times 1)}{\left\{\frac{\partial J}{\partial a}\right\}} = \underset{(m\times m)}{[A(x)]}\underset{(m\times 1)}{\{a(x)\}} - \underset{(m\times n)}{[B(x)]}\underset{(n\times 1)}{\{\delta\}} = \underset{(m\times 1)}{\{0\}}, \tag{6}$$

where $[A(x)]$ and $[B(x)]$ are given by:

$$\underset{(m\times m)}{[A(x)]} = \underset{(m\times n)}{[P]^{\mathrm{T}}}\underset{(n\times n)}{[W(x)]}\ \underset{(n\times m)}{[P]}, \tag{7}$$

$$\underset{(m\times n)}{[B(x)]} = \underset{(m\times n)}{[P]^{\mathrm{T}}}\underset{(n\times n)}{[W(x)]}. \tag{8}$$

From Eq. (6) the vector of the coefficients $\{a(x)\}$ assumes the expression:

$$\underset{(m\times 1)}{\{a(x)\}} = \underset{(m\times m)}{[A(x)^{-1}]}\underset{(m\times n)}{[B(x)]}\underset{(n\times 1)}{\{\delta\}}. \tag{9}$$

By using Eqs. (9) and (1), $\eta(x)$ can be expressed as:

$$\eta(x) = \sum_{I=1}^{n} g_I(x)\delta_I \equiv \underset{(1\times n)}{\{g(x)\}^{\mathrm{T}}}\underset{(n\times 1)}{\{\delta\}}, \tag{10}$$

$\{g(x)\}$ being the vector of the shape functions for the MLS approximation:

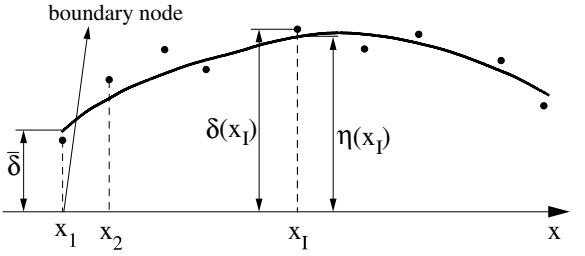

Fig. 2. The approximation function $\eta(x)$ and the nodal values δ. The MLS approximation is such that $\eta(x_I) \neq \delta_I$.

$$\underset{(1\times n)}{\{g(x)\}^{\mathrm{T}}} = [g_1(x), \ldots, g_n(x)] = \underset{(1\times m)}{\{p(x)\}^{\mathrm{T}}}\underset{(m\times m)}{[A(x)^{-1}]}\underset{(m\times n)}{[B(x)]}, \tag{11}$$

where $\{g(x)\}^{\mathrm{T}} = \{g_1, g_2, \ldots, g_n\}$ are the MLS shape functions related to the nodes $x_1, x_2, \ldots, x_n$.

From Eq. (10) it should be noted that, in general, the approximation $\eta(x)$ is such that $\eta(x_I) \neq \delta_I$, Fig. 2. In the following, the MLS shape functions will be used to solve the elastic problem so that Eq. (10) will be applied to each displacement component. The displacement field will be denoted by the vector $\{\eta\}$.

3. Variational formulation

The shape functions derived in the former section are introduced into a variational formulation for a linear elastic solid. Eq. (11) is referred to the approximation of a scalar variable and the vector $\{\delta\}$ has dimension equal to the MLS nodes number, N. For an elastic solid in a n_d–dimensional space, let $\{\eta\}$ be the displacement field, with n_d components and $N_d = n_d N$. The MLS approximation can be applied for each component of the displacement field in the form:

$$\underset{(n_d\times 1)}{\{\eta\}} = \underset{(n_d\times N_d)(N_d\times 1)}{[G_\eta]}\ \underset{}{\{\delta\}}, \tag{12}$$

where $[G_\eta]$ is the matrix of the shape functions and $\{\delta\}$ is the vector of all the nodal components of the approximation variables. For simplifying the notation, we introduce the following shape function vector for the deformations:

$$\underset{(d\times 1)}{\{\varepsilon\}} = \underset{(d\times n_d)(n_d\times 1)}{[\partial]}\ \underset{}{\{\eta\}} = \underset{(d\times n_d)(n_d\times N_d)(N_d\times 1)}{[\partial]}\ \underset{}{[G_\eta]}\ \underset{}{\{\delta\}} = \underset{(d\times N_d)(N_d\times 1)}{[G_\varepsilon]}\ \underset{}{\{\delta\}} \tag{13}$$

with $d = 1$ for $n_d = 1$ and $d = 3 \times (n_d - 1)$ for $n_d = 2, 3$ and $\{\varepsilon\}$ is the deformation vector, while the matrix $[\partial][G_\eta] = [G_\varepsilon]$ is determined by ordering and adding appropriately the derivative of the MLS shape functions.

Let consider the domain Ω of a solid subjected to volume forces $\{F\}$, surface forces $\{q\}$ and prescribed

displacements $\{\bar{\eta}\}$, acting respectively on Ω, $\partial\Omega_q$ and $\partial\Omega_\eta$.

The minimum of the following total potential energy functional corresponds to the elastic problem solution:

$$\begin{aligned}\Pi(\{\eta\}) = {} & \frac{1}{2}\int_\Omega \underset{(1\times n_d)(n_d\times d)(d\times d)(d\times n_d)(n_d\times 1)}{\{\eta\}^{\mathrm{T}}\,[\partial]^{\mathrm{T}}\,[H]\,[\partial]\,\{\eta\}}\,\mathrm{d}\Omega \\ & - \int_\Omega \underset{(1\times n_d)(n_d\times 1)}{\{F\}^{\mathrm{T}}\,\{\eta\}}\,\mathrm{d}\Omega - \int_{\partial\Omega_q} \underset{(1\times n_d)(n_d\times 1)}{\{q\}^{\mathrm{T}}\,\{\eta\}}\,\mathrm{d}S \\ & + \int_{\partial\Omega_\eta} \mathrm{ind}\left(\underset{(n_d\times 1)}{\{\bar{\eta}\}} - \underset{(n_d\times 1)}{\{\eta\}}\right)\mathrm{d}S, \end{aligned} \tag{14}$$

where $\{\eta\} = \{\eta(x,\delta)\}$ is the displacement vector, whose components are given by Eq. (11), and $[H]$ is the elastic operator.

In the paper the evaluation of the integrals appearing in the variational principle, Eq. (14), is obtained through a standard Gaussian quadrature on the domain Ω and by the partition of unity quadrature, described in Section 4. The Gaussian quadrature requires the subdivision of the domain Ω into quadrature subcells by introducing a background mesh. This mesh does not play any role in the approximation and must be chosen to ensure an appropriate evaluation of the integrals.

In the last term of Eq. (14) the indicator function is introduced, defined by:

$$\mathrm{ind}(\{\bar{\eta}\} - \{\eta\}) = \begin{cases} 0 & \text{if } \{\bar{\eta}\} - \{\eta\} = \{0\}, \\ +\infty & \text{if } \{\bar{\eta}\} - \{\eta\} \neq \{0\}. \end{cases} \tag{15}$$

This term is necessary as the MLS shape functions do not satisfy the essential boundary conditions, being $\{\eta(x_I)\} \neq \{\delta_I\}$. In fact, the shape functions $\{g(x)\}$, defined by Eq. (11), take non-zero values for each point included in the influence domain Ω_I of the node x_I. To transform the indicator function into a differentiable equivalent one, it is regularized by the augmented Lagrangian technique [10,11].

If the assigned displacements $\{\bar{\eta}\}$ are interpolated by a set of Dirac delta functions placed at the nodes x_I on $\partial\Omega_\eta$, the following expression is obtained:

$$\begin{aligned} & \int_{\partial\Omega_\eta} \mathrm{ind}(\{\bar{\eta}\} - \{\eta\})\,\mathrm{d}S \\ & = \sum_{i=1}^{n_r} \sup_{\{r\}_i} \Big[\{r\}_i^{\mathrm{T}}(\{\bar{\eta}_r\}_i - \{\eta_r\}_i) \\ & \quad + \frac{1}{2}\alpha(\{\bar{\eta}_r\}_i - \{\eta_r\}_i)^{\mathrm{T}}(\{\bar{\eta}_r\}_i - \{\eta_r\}_i)\Big], \end{aligned} \tag{16}$$

where $\{r\}_i$ and $\{\bar{\eta}_r\}_i$ are, respectively, the reactions (which have the mathematical meaning of Lagrangian multipliers) and the assigned displacements on the n_r constrained nodes, while α is a positive penalty parameter.

By introducing Eq. (16) into Eq. (14), and being:

$$\underset{(N_d\times N_d)}{[K]} = \int_\Omega \underset{(N_d\times d)(d\times d)(d\times N_d)}{[G_\varepsilon]^{\mathrm{T}}\,[H]\,[G_\varepsilon]}\,\mathrm{d}\Omega, \tag{17}$$

$$\underset{(N_d\times 1)}{\{F\}} = \int_\Omega \underset{(N_d\times n_d)(n_d\times 1)}{[G_\eta]^{\mathrm{T}}\,\{F\}}\,\mathrm{d}\Omega + \int_{\partial\Omega_q} \underset{(N_d\times n_d)(n_d\times 1)}{[G_\eta]^{\mathrm{T}}\,\{q\}}\,\mathrm{d}S, \tag{18}$$

the following functional is obtained:

$$\begin{aligned} \Pi(\delta,r) = {} & \frac{1}{2}\underset{(1\times N_d)(N_d\times N_d)(N_d\times 1)}{\{\delta\}^{\mathrm{T}}\,[K]\,\{\delta\}} - \underset{(1\times N_d)(N_d\times 1)}{\{\delta\}^{\mathrm{T}}\,\{F\}} \\ & + \sum_{i=1}^{n_r}\left[\underset{(1\times n_d)}{\{r\}^{\mathrm{T}}}\left(\underset{(n_d\times 1)}{\{\bar{\eta}_r\}} - \underset{(n_d\times N_d)(N_d\times 1)}{[G_\eta]\,\{\delta\}}\right)\right. \\ & + \frac{1}{2}\alpha\left(\underset{(n_d\times 1)}{\{\bar{\eta}_r\}} - \underset{(n_d\times N_d)(N_d\times 1)}{[G_\eta]\,\{\delta\}}\right)^{\mathrm{T}} \\ & \left.\times\left(\underset{(n_d\times 1)}{\{\bar{\eta}_r\}} - \underset{(n_d\times N_d)(N_d\times 1)}{[G_\eta]\,\{\delta\}}\right)\right]_i. \end{aligned} \tag{19}$$

Introducing a suitable shape function matrix $[Q_b]$, defined by:

$$\underset{(n_d n_r\times N_d)}{[Q_b]} = \begin{bmatrix} [G_\eta]_1 \\ [G_\eta]_2 \\ \cdots \\ [G_\eta]_{n_r} \end{bmatrix}, \tag{20}$$

the functional in Eq. (19) can be written in the following form:

$$\begin{aligned} \Pi(\delta,r) = {} & \frac{1}{2}\underset{(1\times N_d)(N_d\times N_d)(N_d\times 1)}{\{\delta\}^{\mathrm{T}}\,[K]\,\{\delta\}} - \underset{(1\times N_d)(N_d\times 1)}{\{\delta\}^{\mathrm{T}}\,\{F\}} \\ & + \underset{(1\times n_r n_d)}{\{r\}^{\mathrm{T}}}\left(\underset{(n_r n_d\times 1)}{\{\bar{\eta}_r\}} - \underset{(n_r n_d\times N_d)(N_d\times 1)}{[Q_b]\,\{\delta\}}\right) \\ & + \frac{1}{2}\alpha\left(\underset{(n_r n_d\times 1)}{\{\bar{\eta}_r\}} - \underset{(n_r n_d\times N_d)(N_d\times 1)}{[Q_b]\,\{\delta\}}\right)^{\mathrm{T}} \\ & \times\left(\underset{(n_r n_d\times 1)}{\{\bar{\eta}_r\}} - \underset{(n_r n_d\times N_d)(N_d\times 1)}{[Q_b]\,\{\delta\}}\right) \end{aligned} \tag{21}$$

whose saddle-point is the elastic problem solution:

$$\min_{\{\delta\}}\max_{\{r\}}\Pi(\delta,r). \tag{22}$$

In the last formula, the superior extremum has been substituted by the maximum, in the hypothesis of a well posed elastic problem.

The present variational formulation, named augmented Lagrangian element free (ALEF) [10], allows to eliminate all the drawbacks related to the use of the Lagrangian and penalty methods and represents a computationally effective approach for the introduction

of constrains on direct variables in the MLS approximation [10].

4. The partition of unity quadrature method

In this section, the quadrature method for the weak form of the equilibrium equations is introduced. A more detailed analysis of the method is presented in [7]. This method will be called partition of unity quadrature (PUQ), as it is conceptually based on the partition of unity property of the MLS shape functions [6]. This property states that at any point of the domain the MLS shape functions given by Eq. (11) are such that [9,12]:

$$\sum_{I=1}^{n} g_I(x) = 1, \quad \forall x \in \Omega. \tag{23}$$

To this end let f an integrable function defined over the domain Ω. In the same domain a set of N MLS nodes is considered, and the relevant shape functions g_I, $I = 1, \ldots, N$, are computed.

Let Ω_I be the support for the weight function g_I, and Ξ, the function indicating if a generic point x is located inside the domain Ω, be defined by:

$$\Xi(x) = \begin{cases} 1 & \text{if } x \in \Omega, \\ 0 & \text{if } x \notin \Omega. \end{cases} \tag{24}$$

The MLS shape function g_I is defined on the support of the weight function for the node x_I, as follows from Eqs. (11) and (2). Its domain of definition can be easily extended to the whole domain Ω by:

$$g_I(x) = \begin{cases} g_I(x) & \text{if } x \in \Omega_I, \\ 0 & \text{if } x \notin \Omega_I. \end{cases} \tag{25}$$

Observing that $g_I(x) = 0$, $\forall x \notin \Omega_I$, and that the value of the integral does not change if the integrand function is multiplied by one it follows:

$$\int_\Omega f \, \mathrm{d}\Omega = \int_\Omega f \sum_{I=1}^{n} g_I \, \mathrm{d}\Omega = \sum_{I=1}^{N} \int_{\Omega_I} f \Xi g_I \, \mathrm{d}\Omega. \tag{26}$$

This equation is the basis of the PUQ method and it states that it is possible to evaluate any integral subdividing the total domain into the union of the weight function supports, and evaluate the integral as the sum of the integrals computed within each support weighting the integrand function by the MLS shape function associated with the support. The function Ξ cuts the supports if they extend outside the domain Ω, as happens when the supports intersect the boundary $\partial\Omega$.

The PUQ method can be used in the evaluation of definite integrals without any connection with element-free methods by generating a cloud of points for the construction of the partition of unity. Its application rises naturally in element-free methods, where a set of points and associated supports is fixed for constructing the shape functions, and it can be conveniently used at the same time for applying the PUQ.

The fundamental feature of the PUQ method is, therefore, that there is no need to introduce a background quadrature mesh since the quadrature cells are determined by the weight supports themselves, and there is no need to modify the variational formulation as suggested by Atluri and Zhu in the MLPG [5]. Moreover, as observed by Dolbow and Belytschko [13], the coincidence between quadrature cells and weight supports reduces the error in the integral evaluation. Finally, it should be noted that there is no need for the MLS shape functions and for the partition of unity weight functions g_I, Eq. (26), to coincide, and they can be constructed with respect to different bases and weights. This observation is particularly noteworthy when enriched bases are used for the approximation, as the presence of the weight function in the integral makes it more difficult to be evaluated. Therefore, it seems a good idea to assume the simplest basis and weights for determining the partition of unity quadrature weight function.

A key point in the application of the method is the quadrature rule adopted in each support. When the support is circular and fully contained in Ω, specific quadrature formulas [14,15] can be used. If the support is cut by the boundary of Ω, it can be subdivided into quadrature subdomains made by triangles and circular sectors, Fig. 3. This problem has been considered [4] and solved by introducing quadrature subcells that are mapped onto a unit circle, Fig. 3b. Here a slightly different approach is followed. After the division in subcells is made, four basic regions are generated: triangles, quadrilaterals, polar triangles (two sides linear and one side circular) and polar rectangles (two sides linear and two sides circular), Fig. 3a, mapped as follows [15]:

- triangles onto two-dimensional simplex (T);
- quadrilaterals, polar triangles, polar rectangles onto square (C).

In the elementary regions (T) and (C), a seventh order formula is used [7,15]. The PUQ has been implemented for both circular and rectangular supports. If rectangular supports are used, the support is of course subdivided into triangles and quadrilaterals, or simply quadrilaterals, and no polar type cells are generated.

Actually, in the numerical tests carried out to estimate the stress intensity factors, no advantage has been observed in considering the intersection of the supports with the external boundary or the crack surface. Considering the intersection reintroduces in some way a local "meshing" of the support, as its standard shape is modified. Alternatively, the integrand function is assumed equal to zero if the quadrature point lies outside

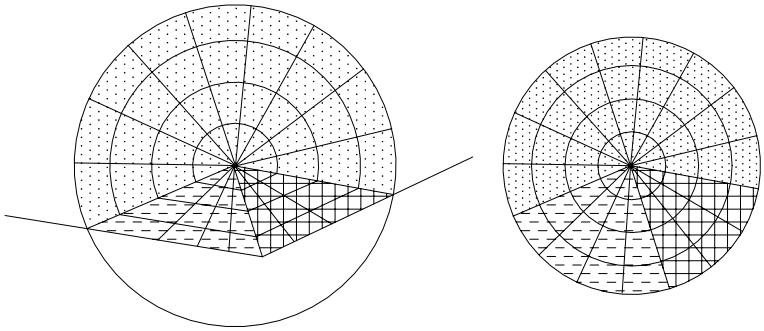

Fig. 3. (a) Support cut by the boundary and (b) equivalent mapping on the unit circle for triangle and quadrilateral quadrature formulas.

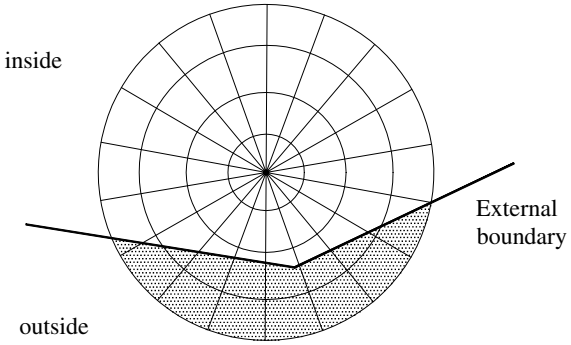

Fig. 4. Support cut by the boundary.

the domain of the body, Fig. 4. In this way the quadrature points and weights are fixed for the standard support, and the method is completely mesh free.

5. Virtual crack model

One of the most important properties of the MLS approximation is the ability to produce solutions with the desired degree of continuity. In fact the MLS approximation inherits its continuity and differentiability properties both from the basis functions and from the weight functions.

Although high continuity is often a desiderable property, material interfaces and cracks deserve special treatment for the presence of discontinuous quantities in the solution. The treatment of crack discontinuities in a solid has been analyzed in several ways [16]. A first basic approach, known as *visibility criterion*, considers the crack line as opaque for the weight functions and the support takes the shape illustrated in Fig. 5a. As a consequence, a discontinuity in the weight and shape functions is introduced, not only on the crack line, but also in the interior of the domain Ω. Such a discontinuity is introduced for each weight function whose support contains the crack tip, so that the final solution is discontinuous and oscillatory near the tip.

A more refined approach, called *diffraction method*, applies only to polar-type weight functions (i.e. with circular support) and is based on the evaluation of the distance by a path which passes around the tip, Fig. 5b. Consequently, the weight and the shape functions are discontinuous across the crack, but continuous and differentiable elsewhere. This approach leads, however,

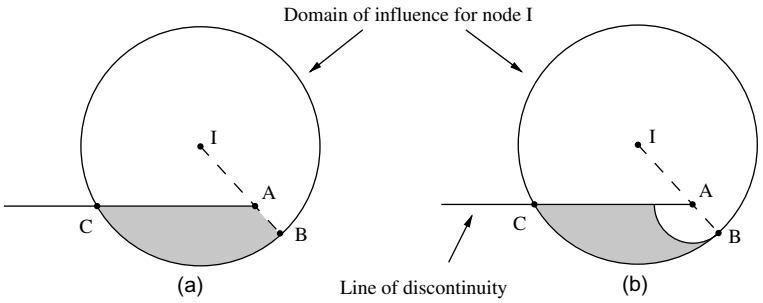

Fig. 5. Domains of influence of nodes adjacent to a line of discontinuity: (a) visibility criterion and (b) diffraction method. The shaded regions are removed from the domain of influence.

to quite complex shape functions with rapidly varying derivatives, so the quadrature of the variational form can present difficulties [16].

A recent approach in the treatment of discontinuities both in meshless and in the finite element method is based on the introduction of discontinuous enrichment functions in the approximation bases. Within this approach some additional variables are introduced in the nodes close to the discontinuity, playing the role of coefficients for the discontinuous functions. This approach is going to substitute completely the visibility and diffraction methods [17,18].

In previous papers [19,20], a different approach for modelling the crack discontinuity has been presented. It preserves the continuity of the solution in Ω, does not introduce any weight support modification or enrichment and is computationally effective. As pointed out in Section 3, the ALEF approach [10] allows the introduction of Lagrangian multipliers in a computationally effective framework. To take advantage from this property, the proposed model is based on the imposition of suitable interface conditions through Lagrangian multipliers.

The crack is virtually extended in the direction of the tangent at the tip, Fig. 6. All the weight functions whose supports intersect the real crack are cut along the crack line (real + virtual), while the weight functions whose supports intersect only the virtual crack are left unchanged. If D_{L} and D_{R} are the two sides of the crack, y_C is the real crack tip and I is a generic point of the discretization whose weight function has radius r_I, the model is such that:

- if $|x_I - y_C| > r_I$, the weight function is left unchanged;
- if $I \in D_{\mathrm{L}}$ and $r_I > |x_I - y_C|$, then $w_I = 0\ \forall x \in D_{\mathrm{R}}$;
- if $I \in D_{\mathrm{R}}$ and $r_I > |x_I - y_C|$, then $w_I = 0\ \forall x \in D_{\mathrm{L}}$.

This model introduces of course a discontinuity along the virtual crack because of the weight function cutting. The discontinuity can be suppressed introducing a suitable number of interface points on the two sides of the virtual crack. Each interface point is given by two coincident points, one belonging to D_{L} and the other belonging to D_{R}, subjected to the following interface conditions:

$$\{\eta_L\} = \{\eta_R\}, \quad \forall I \in \Gamma_{\mathrm{VC}}, \tag{27}$$

$$\{\varepsilon(\eta_L)\} = \{\varepsilon(\eta_R)\}, \quad \forall I \in \Gamma_{\mathrm{VC}}, \tag{28}$$

Γ_{VC} being the virtual crack.

The length of the virtual crack must be, in general, greater than the maximum diameter of the weight functions in the neighbor of the tip and a symmetric arrangement of nodes around the tip is recommended. The model ensures:

- well-defined MLS approximation in the whole domain;
- the representation of discontinuous displacements over the crack;
- the continuity of the solution in the whole domain;
- the absence of mutual influences for nodes belonging to different sides of the crack.

Moreover the virtual crack model allows for a simple introduction of a cohesive law at the crack interface. By considering the MLS expressions for displacements and deformations, the interface conditions assume the following form:

$$\left(\underset{(n_d \times N_d)}{[G_\eta^{(L)}]} - \underset{(n_d \times N_d)}{[G_\eta^{(R)}]} \right)_i \underset{(N_d \times 1)}{\{\delta\}} = \underset{(n_d \times 1)}{\{0\}}, \quad i = 1, \ldots, n_\Gamma, \tag{29}$$

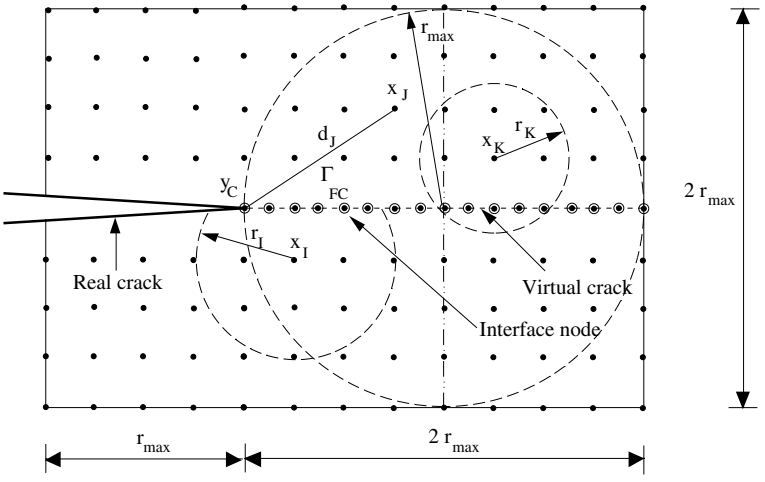

Fig. 6. The virtual crack model for simulating the crack discontinuity.

$$\left(\underset{(d\times N_d)}{[G_\varepsilon^{(L)}]} - \underset{(d\times N_d)}{[G_\varepsilon^{(R)}]} \right)_i \underset{(N_d\times 1)}{\{\delta\}} = \underset{(d\times 1)}{\{0\}}, \quad i = 1,\ldots,n_\Gamma. \tag{30}$$

The interface conditions for both displacements and deformations for all the n_Γ interface nodes are therefore linear constraints on the approximation variables, and they can be written in the following matrix form:

$$\underset{(n_d n_\Gamma \times N_d)(N_d\times 1)}{[Q_\eta]} \underset{(n_d n_\Gamma \times 1)}{\{\delta\}} = \underset{(n_d n_\Gamma \times 1)}{\{0\}}, \tag{31}$$

$$\underset{(dn_\Gamma \times N_d)(N_d\times 1)}{[Q_\varepsilon]} \underset{(dn_\Gamma \times 1)}{\{\delta\}} = \underset{(dn_\Gamma \times 1)}{\{0\}}, \tag{32}$$

where the constraint matrix $[Q_\eta]$ has dimension $(n_d n_\Gamma) \times (N_d)$, for each node displacement vector having n_d components, while $[Q_\varepsilon]$ has dimension $(dn_\Gamma) \times (N_d)$.

The discretized augmented Lagrangian functional is extended to the present problem by adding the term:

$$\{r_\Gamma\}^{\mathrm{T}}[Q_\eta]\{\delta\} + \tfrac{1}{2}\alpha([Q_\eta]\{\delta\})^{\mathrm{T}}([Q_\eta]\{\delta\}) + \tag{33}$$

$$+\{\sigma_\Gamma\}^{\mathrm{T}}[Q_\varepsilon]\{\delta\} + \tfrac{1}{2}\beta([Q_\varepsilon]\{\delta\})^{\mathrm{T}}([Q_\varepsilon]\{\delta\}),$$

The total Hessian of the potential energy functional with respect to the approximation variables is given by:

$$\nabla^2_{\delta\delta}\Pi(\{\delta\},\{r\},\{r_\Gamma\},\{\sigma_\Gamma\}) = [K] + \alpha([K_b] + [K_\eta]) + \beta[K_\varepsilon] \tag{34}$$

where the Hessians $[K_b] = [Q_b]^{\mathrm{T}}[Q_b]$ of the boundary conditions and of the material continuity constraints $[K_\eta] = [Q_\eta]^{\mathrm{T}}[Q_\eta]$, $[K_\varepsilon] = [Q_\varepsilon]^{\mathrm{T}}[Q_\varepsilon]$ have been evidenced. All of them are semi-definite positive because they are evaluated by the dyadic product of the constraint matrices $[Q]$. The saddle point of the functional corresponds to the MLS solution of the crack discontinuity problem:

$$\min_{\{\delta\}} \max_{\{r\},\{r_\Gamma\},\{\sigma_\Gamma\}} \Pi(\{\delta\},\{r\},\{r_\Gamma\},\{\sigma_\Gamma\}). \tag{35}$$

The numerical solution can be determined by using the augmented Lagrangian algorithm and the application of the iterative formula by Hestenes and Powell (HP) [21] for all the three sets of Lagrangian multipliers:

minimization w.r.t. the approximation variables $\{\delta\}$:

$$\{\delta^{(k+1)}\} = \arg\min_{\{\delta\}} \Pi\Big(\{\delta\},\{r^{(k)}\},\{r_\Gamma^{(k)}\},\{\sigma_\Gamma^{(k)}\}\Big), \tag{36}$$

HP formulas for the Lagrangian multipliers:

$$\begin{aligned} \{r^{(k+1)}\} &= \{r^{(k)}\} + \alpha\Big(\{\bar{\eta}_r\} - [Q_b]\{\delta^{(k+1)}\}\Big), \\ \{r_\Gamma^{(k+1)}\} &= \{r_\Gamma^{(k)}\} + \alpha[Q_\eta]\{\delta^{(k+1)}\}, \\ \{\sigma_\Gamma^{(k+1)}\} &= \{\sigma_\Gamma^{(k)}\} + \beta[Q_\varepsilon]\{\delta^{(k+1)}\}, \end{aligned} \tag{37}$$

and the choice of an incremental scheme for both penalty parameters α and β [10,21]. The iteration in Eqs. (36) and (37) works alternatively on the variables $\{\delta\}$ and on the Lagrangian multipliers $\{r\}$, $\{r_\Gamma\}$, $\{\sigma_\Gamma\}$. It should be observed in fact that the functional minimum with respect to $\{\delta\}$ is calculated by keeping the values of the multipliers fixed, which are updated at the subsequent step.

The importance of the correct selection of the penalty parameters α and β in the present formulation has been evidenced in previous papers [10,20]. From a theoretical point of view the algorithm will converge for any positive value of the penalty parameters, but in practice the numerical experiments carried out have shown that the selection of appropriate values is not a trivial task. In [10] an efficient algorithm for computing the initial penalty parameter values has been proposed. This algorithm can be straightforwardly extended to crack and interface problems [19]. Let recall the Hessian expression, Eq. (34). The matrices $[K]$, $[K_b]$, $[K_\eta]$, $[K_\varepsilon]$ are summed up weighted by the penalty coefficients. To ensure the best numerical conditioning of the problem the spectral radii of the matrices must be properly scaled.

These matrices are all positive semidefinite, and therefore their minimum eigenvalue can be assumed in general equal to zero. Before starting the augmented Lagrangian iteration the following maximum eigenvalues are estimated:

$$\lambda_K = \max \mathrm{eig}[K], \tag{38}$$

$$\lambda_b = \max \mathrm{eig}[K_b], \tag{39}$$

$$\lambda_\eta = \max \mathrm{eig}[K_\eta], \tag{40}$$

$$\lambda_\varepsilon = \max \mathrm{eig}[K_\varepsilon], \tag{41}$$

and the initial penalty parameters are set as follows:

$$\alpha = \frac{\lambda_K}{10\min(\lambda_b,\lambda_\eta)}, \qquad \beta = \frac{\lambda_K}{10\lambda_\varepsilon}. \tag{42}$$

Eq. (42) fix the penalty parameter values in such a way that the spectral radii of the matrices $[K]$, $[K_b]$, $[K_\eta]$, $[K_\varepsilon]$ are all comparable. As noticed before, α controls boundary constraints and virtual crack interface displacements, so that the eigenvalues λ_b and λ_η will be of the same order of magnitude.

Some results about the convergence behavior of the augmented Lagrangian algorithm for different values of the penalty parameter α are reported in [10].

6. Numerical examples

In the present section the results produced by standard Gaussian quadrature and partition of unity quadrature are discussed. Attention is focused on the evaluation of the stress intensity factors, as they are the

quantities determining the crack trajectory when the maximum stress criterion for crack propagation is used. No propagating crack examples are given due to current software limitation, as the translation of the virtual crack interface is actually not implemented.

A flat sheet in tension is examined considering first an orthogonal edge crack (pure mode I), and then a slant edge crack (mixed mode). Both examples are modelled in plane stress state using the linear basis, enriched by the $\sqrt{r}$ function:

$$\{p\}^{\mathrm{T}} = \{1, x, y, \sqrt{r}\}, \tag{43}$$

r being the distance from the crack tip. The exponential weight function:

$$w(d) = \begin{cases} \dfrac{\mathrm{e}^{-(d/c)^{2k}} - \mathrm{e}^{-(d_m/c)^{2k}}}{1 - \mathrm{e}^{-(d_m/c)^{2k}}} & d \leqslant d_m, \\ 0 & d > d_m, \end{cases} \tag{44}$$

has been used, with $k = 1$, $d_m/c = 5$ and a radius d_m of the supports containing a number of MLS nodes equal to 7 times the number of the basis functions, i.e. 28 nodes.

The first example is illustrated in Fig. 7. For this example the MLS discretization is reported in Fig. 8, where the nodes surrounded by a circle are the virtual crack interface nodes and the ones surrounded by a square are the edge crack nodes. Fig. 9 reports the quadrature cells used for the standard Gaussian quadrature. The stress intensity factor K_{I} has been evaluated by the decomposition method, using circular J-integral evaluation paths centered at the crack tip. The method is described in [22], along with a boundary elements code, here used for comparison in the assessment of the results.

The data used in the example are $a = 1$, $\sigma = 1$ with elastic constants $E = 10^5$, $\nu = 0.3$. The "exact" solution of the problem, is $K_{\mathrm{I}} = 2.38$. It should be noted that the use of the enhanced basis, Eq. (43), makes impossible the enforcement of the deformation continuity at the crack tip interface, as infinite values arise. This inconvenient has been circumvented by introducing a couple

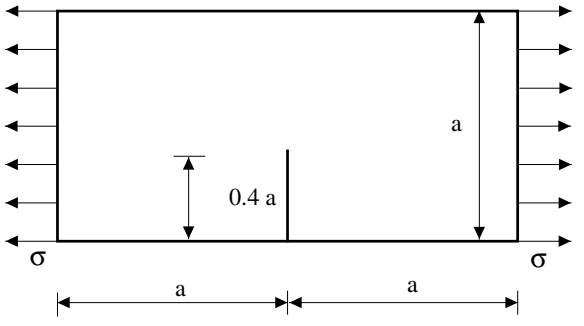

Fig. 7. Mode I edge crack example.

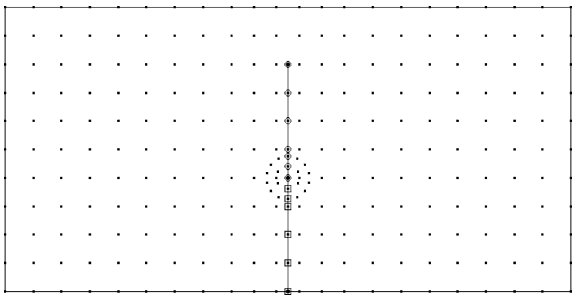

Fig. 8. MLS and interface nodes for the orthogonal edge crack example.

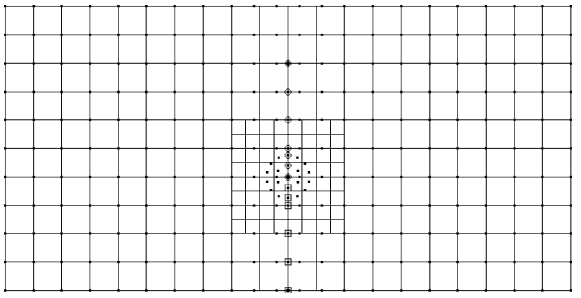

Fig. 9. Background quadrature cells for the orthogonal edge crack problem.

of interface nodes immediately ahead the crack tip. At the crack tip only the displacement continuity is therefore constrained.

The second example is illustrated in Fig. 10. The edge crack has length equal to $0.5a$, slanted by $\pi/4$ with respect to the lower edge of the model. The MLS nodes and the integration cells are reported respectively in Figs. 11 and 12. The reference results for this example are $K_{\mathrm{I}} = 1.50$, $K_{\mathrm{II}} = 0.72$.

In both cases the reference "exact" values for the stress intensity factors have been evaluated by the BEM code [22] and verified with the handbook [23], while the values computed by the present model have been computed with reference to a J-integral circular path having

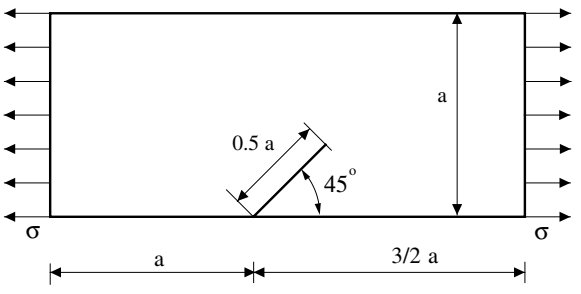

Fig. 10. Slant edge crack problem.

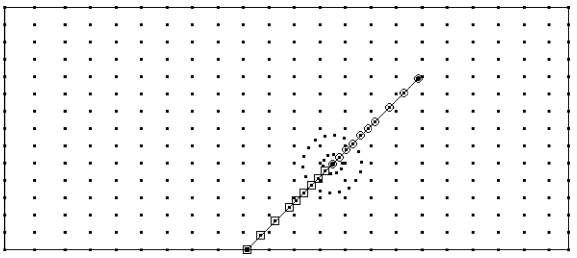

Fig. 11. MLS and interface nodes for the slant edge crack example.

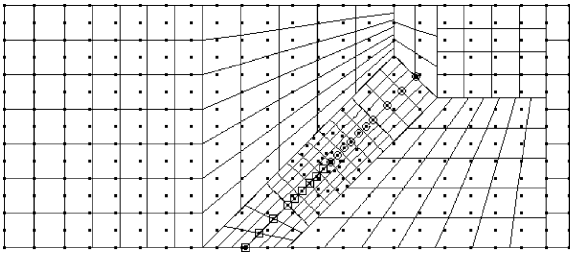

Fig. 12. Background quadrature cells for the slant edge crack problem.

radius equal to 0.3 times the crack length. The presented results have been verified for being substantially independent from the number and disposition of the nodes at the virtual crack interface. The results comparing the stress intensity factors for both standard Gaussian and partition of unity quadratures are reported in Tables 2 and 3. In the tables different partition of unity weights are used, by constructing MLS shape functions with respect to different bases for the approximation and for the quadrature, Eq. (26), in such a way the integrand function is simplified. Three cases has been considered, each one using as PUQ weight:

- the same shape functions constructed for the approximation;
- MLS shape functions constructed with the exponential weight function and the Shephard's basis, formed only by the constant term, $\{p\}^{\mathrm{T}} = \{1\}$;
- MLS shape functions constructed with the linear conical weight function [9] and the Shephard's basis.

The latter approach proves effective when large supports and support subdivisions are used [6,7], like in the present applications, where each circular support has been subdivided into six polar triangles having vertex at the center of the circle and a seventh order quadrature formula with 16 Gauss points in each triangle. In fact considering both the evaluation of the stress intensity factors and the area of the domain, evaluated for checking the PUQ in the integration of the unit function to have a simple measure of the performance of the method, it is apparent that the use of the simplest PUQ weight improves significantly the result. The percentage error of approximation, defined by

$$E(r) = 100 \times \frac{|r_{\mathrm{exact}} - r_{\mathrm{num}}|}{r_{\mathrm{exact}}} \tag{45}$$

r being a quantity of interest, is reported in Tables 2 and 3 as well.

Table 2
Comparison of the results for the mode I example

	K_{I}	$E(K_{\mathrm{I}})$ (%)	Quadrature points	Domain area	E(area) (%)
Exact result	2.38	0.00	–	2.00	0.00
Standard Gaussian	2.31	2.94	9344	–	–
PUQ, shape functions	2.33	2.10	20548	1.87	6.50
PUQ, Shephard	2.44	2.52	20548	1.83	8.50
PUQ, Shephard, conical	2.32	2.52	20548	2.01	0.50

Table 3
Comparison of the results for the mixed mode example

	K_{I}	$E(K_{\mathrm{I}})$ (%)	K_{II}	$E(K_{\mathrm{II}})$ (%)	Quadrature points	Domain area	E (area) (%)
Exact result	1.50	0.00	0.72	0.00	–	2.50	0.00
Standard Gaussian	1.56	4.00	0.74	2.78	9180	–	–
PUQ, shape functions	1.59	6.00	0.69	4.17	33880	2.45	2.00
PUQ, Shephard	1.70	13.33	0.82	13.89	33880	2.12	15.20
PUQ, Shephard, conical	1.50	0.00	0.74	2.78	33880	2.50	0.00

The results show that the PUQ can be accurate as the Gaussian quadrature, but the computing time in the current implementation is higher. The reason for this, explained in [6,7], is basically due to the fact that the discrete form of Eq. (26) does not hold strictly if each support does not cover the entire domain. In this case the PUQ is as fast as the standard Gaussian quadrature, and can produce even more precise results. An improvement of the results can be obtained by using specialized formulas for circular domains [14]. Some studies on this point are currently carried out. A straightforward and simple conclusion from these results could be to adopt the PUQ in a subregion near the crack tip, using weight supports covering the entire subregion, and standard Gaussian quadrature in the remaining part of the domain. This can be useful for avoiding the generation of a very fine integration cell structure near the crack tip.

In both numerical examples the augmented Lagrangian iteration has performed very well despite of the fact that the problem constraints are very differently scaled. Using the proposed method for the evaluation of the initial penalty parameters, a displacement convergence tolerance equal to 10^{-6} and a strain convergence tolerance equal to 10^{-8}, the solution has been found in a few iterations consuming a very small fraction of the total computing time. In practical computations it has been noticed that the manual selection of the penalty parameters is almost impossible and very inefficient [20]. The proposed algorithm for their automatic evaluation not only has always converged, but reduces substantially the total number of iterations.

7. Conclusions

The paper presents a new approach for the computation of the quadrature of the variational form related to a MLS meshless formulation. Based on the partition of unity property of the moving least squares shape functions, the integrals on the whole domain are substituted by the sum of integrals over standard supports, eliminating in this way the need for a background quadrature mesh. This approach appears especially useful whenever the problem discretization evolves, like in fracture mechanics problems.

The crack discontinuity is modelled by the virtual crack model, based on the introduction of interface conditions in a zone ahead the crack tip, and on the augmented Lagrangian solution of the resulting problem. Some numerical examples about the evaluation of stress intensity factors illustrate the effectiveness of the partition of unity quadrature, although some further development is needed to improve its numerical efficiency.

References

[1] Babuška I, Melenk JM. The partition of unity finite element method: Basic theory and application. Comput Meth Appl Mech Eng 1996;139:289–314.
[2] Beissel S, Belytschko T. Nodal integration of the element free Galerkin method. Comput Meth Appl Mech Eng 1996;139:49–74.
[3] Chen JS, Wu CT, Yoon S, You Y. A stabilized conforming nodal integration for Galerkin meshfree methods. Int J Num Meth Eng 2001;50(2):435–66.
[4] Atluri SN, Zhu T. A new meshless local Petrov–Galerkin (MLPG) approach in computational mechanics. Comput Mech 1998;22:117–27.
[5] Atluri SN, Zhu T. New concepts in meshless methods. Int J Num Meth Eng 2000;47:537–56.
[6] Carpinteri A, Ferro G, Ventura G. Partition of unity weighted quadrature in meshless methods. In: Waszczyszyn Z, Pamin J, editors. Proceedings European Conference on Computational Mechanics ECCM 2001. Cracow, Poland: Fundacja Zdrowia Publicznego; 2001.
[7] Carpinteri A, Ferro G, Ventura G. The partition of unity quadrature in meshless methods. Int J Num Meth Eng 2002;54:987–1006.
[8] Belytschko T, Gu L, Lu YY. Fracture and crack growth by element-free Galerkin methods. Model Simul Mater Sci Eng 1994;2:519–34.
[9] Belytschko T, Krongauz Y, Organ D, Fleming M, Krysl P. Meshless methods: an overview and recent developments. Comput Meth Appl Mech Eng 1996;139:3–47.
[10] Ventura G. An augmented Lagrangian approach to essential boundary conditions in meshless methods. Int J Num Meth Eng 2002;53(4):825–42.
[11] Cuomo M, Ventura G. Complementary energy formulation of no-tension masonry-like solids. Comput Meth Appl Mech Eng 2000;189:313–39.
[12] Melenk JM, Babuška I. The partition of unity method. Int J Num Meth Eng 1997;40:727–58.
[13] Dolbow J, Belytschko T. Numerical integration of the Galerkin weak form in meshfree methods. Comput Mech 1999;23:219–30.
[14] Engels H. Numerical Quadrature and Cubature. London: Academic Press; 1980.
[15] Stroud AH. Approximate Calculation of Multiple Integrals. Englewood Cliffs, NJ: Prentice Hall; 1971.
[16] Organ D, Fleming M, Terry T, Belytschko T. Continuous meshless approximations for nonconvex bodies by diffraction and transparency. Comput Mech 1996;18:1–11.
[17] Belytschko T, Moës N, Usui S, Parimi C. Arbitrary discontinuities in finite elements. Int J Num Meth Eng 2001;50(4):993–1013.
[18] Ventura G, Xu JX, Belytschko T. A vector level set method and new discontinuity approximations for crack growth by EFG. Int J Num Meth Eng 2002;54(6):923–44.
[19] Carpinteri A, Ferro G, Ventura G. Material and crack discontinuities: application of an element free augmented Lagrangian method. In: Brebbia CA, Carpinteri A, editors. Damage and fracture mechanics. Southampton, UK: Computational Mechanics Publications; 1998. p. 237–46.

[20] Carpinteri A, Ferro G, Ventura G. An augmented Lagrangian element free (ALEF) approach for crack discontinuities. Comput Meth Appl Mech Eng 2001;191:941–57.
[21] Fletcher R. Practical methods of optimization. New York: Wiley; 1987.
[22] Portela A, Aliabadi MH. Crack growth analysis using boundary elements. Southampton, UK, Boston, USA: Computational Mechanics Publications; 1992.
[23] Sih GC. Handbook of stress intensity factors. Bethlehem: Leigh University; 1973.